A&A 524, A97 (2010)
DOI: 10.1051/0004-6361/201015306

Astronomy & Astrophysics

Deep *XMM-Newton* observation of the η Chamaeontis cluster⋆,⋆⋆

J. López-Santiago[1], J. F. Albacete Colombo[2], and M. A. López-García[1]

[1] Departamento de Astrofísica y Ciencias de la Atmósfera, Universidad Complutense de Madrid, 28040 Madrid, Spain
e-mail: [jls;mal]@astrax.fis.ucm.es
[2] Centro Universitario Regional Zona Atlántica (CURZA) Universidad Nacional del COMAHUE, Monseñor Esandi y Ayacucho (8500), Viedma (Rio Negro), Argentina
e-mail: donfaca@gmail.com

Received 30 June 2010 / Accepted 6 September 2010

ABSTRACT

Context. The members of the η Chamaeontis cluster are in an evolutionary stage in which disks are rapidly evolving. It also exhibits some peculiarities, such as the large fraction of binaries and accretion disks, probably related to the cluster formation process. Its proximity makes this stellar group an ideal target for studying the relation between X-ray emission and those stellar parameters.
Aims. Our main objective is to determine the general X-ray properties of the cluster members in terms of coronal temperature, column density, emission measure, X-ray luminosity, and variability. We also aim to establish the relation between the X-ray luminosity of these stars and other stellar parameters, such as effective temperature, binarity, and the presence of accretion disks. Finally, a study of flare energies in each flare event detected during the observations and their relation with some stellar parameters is also performed.
Methods. We used proprietary data from a deep *XMM-Newton* EPIC observation targeting the core of the η Chamaeontis cluster. Specific software for the reduction of *XMM-Newton* data was used to analyze our observation. To detect sources in the composed EPIC pn+mos image, we used the wavelet-based code *PWDetect*. General coronal properties were derived from plasma model fitting. X-ray light curves in the 0.3−8.0 keV energy range were generated for each star.
Results. We determine both the coronal properties and variability of the η Chamaeontis members in the *XMM-Newton* EPIC field-of-view. A total of six flare-like events are clearly detected in five different stars. For them, we derived coronal properties during the flare events and pseudo-quiescent state separately. In our observations, stars that experienced a flare event have higher X-ray luminosities in the pseudo-quiescent state than cluster members of similar spectral type that exhibit no evidence of flaring independently of whether they have an accretion disk or not. Observed flare energies are typical of both pre-main- and main-sequence M stars. We detected no difference between flare energies of stars with and without an accretion disk.

Key words. open clusters and associations: individual: η Chamaeontis – stars: pre-main sequence – stars: coronae – stars: flare – X-ray: stars

1. Introduction

The η Chamaeontis cluster (hereafter η Chamaeontis), named after the eponymous B8V star η Cha, was discovered by Mamajek et al. (1999) using *ROSAT* data. The authors proposed thirteen members, twelve of them being X-ray sources. They later investigated the main properties of the sources (Mamajek et al. 2000) and established a connection between the η Chamaeontis cluster and the ϵ Chamaeontis stellar association (Frink et al. 1998). Both are part of a number of nearly coeval stellar groups that include the TW Hya association and probably originated in the molecular complex Scorpius-Centaurus (see Mamajek et al. 2000). Its proximity and low stellar density ensures that the η Chamaeontis cluster is an unique scenario in the solar vicinity.

With an age of 6−8 Myr, η Chamaeontis presents some particularities. Its members are in an evolutionary stage in which disks are rapidly evolving (see Table 1) and can provide additional constraints on inner disk lifetimes (Haisch et al. 2005; Jayawardhana et al. 2006). It has been found that several cluster members are in fast transition from classical T-Tauri stars (CTTSs) to debris disks (Megeath et al. 2005; Sicilia-Aguilar et al. 2009). The binary fraction observed in the cluster is twice as high as that found for field stars and dense clusters (Lyo et al. 2004), but similar to the binary fraction in Taurus. This result may suggest that there is a relation between the binary fraction and the stellar density of star-forming regions. Some studies of the initial mass function (IMF) of η Chamaeontis (e.g. Moraux et al. 2007) indicate that the cluster mass function exhibits a deficit of low mass stars and brown dwarfs. Nevertheless, Luhman (2004) indicates that other low-mass star-forming regions such as Taurus have very few or no brown dwarfs in stellar samples similar to η Chamaeontis. However, the deficit of low mass stars in the cluster remains unknown. Using numerical simulations, Moraux et al. (2007) concluded that the IMF is typical of clusters formed from a compact configuration and that dynamical interactions can result in the loss of the original cluster members. At the age of η Chamaeontis, stars ejected in the early phases of cluster formation might reach distances of 6 to 10 pc from the cluster center. Thus, one should look for these ejected members at angular distances up to 5 degrees from the

⋆ This publication makes use of data products from the Two Micron All Sky Survey, which is a joint project of the University of Massachusetts and the Infrared Processing and Analysis Center/California Institute of Technology, funded by the National Aeronautics and Space Administration and the National Science Foundation.
⋆⋆ Appendices are only available in electronic form at http://www.aanda.org

Table 1. Spectral type, binarity, and disk properties of η Chamaeleontis members in the *XMM-Newton* field of view.

Source	RECX	Sp.T.*	Binarity**	Disk type†	log L_{bol}‡ (erg s^{-1})
η Cha	2	B8	?	debris	35.5
EH Cha	3	M3		TO	32.7
EI Cha	4	M1		TO	32.9
EK Cha	5	M4		TO	32.6
EL Cha	6	M3			32.7
EM Cha	7	K6	K6.9+M1.0		33.4
RS Cha	8	A7 + A8	eclipsing		34.9
EN Cha	9	M4	M4.4 + M4.7	TO	32.6
EO Cha	10	M0			33.2
EP Cha	11	K6		class II	33.4
EQ Cha	12	M3	M3.2+M3.2:		32.7
HD 75505	13	A1			35.1
ES Cha	14	M5		TO	32.1
ET Cha	15	M3		class II	32.7

Notes. (*) Torres et al. (2008). (**) Sicilia-Aguilar et al. (2009), determined from Lyo et al. (2004). (†) Sicilia-Aguilar et al. (2009). TO are transitional disk objects. (‡) Luminosities determined from the spectral type, assuming an age of 6 Myr and the Siess et al. (2000)'s pre-main-sequence model.

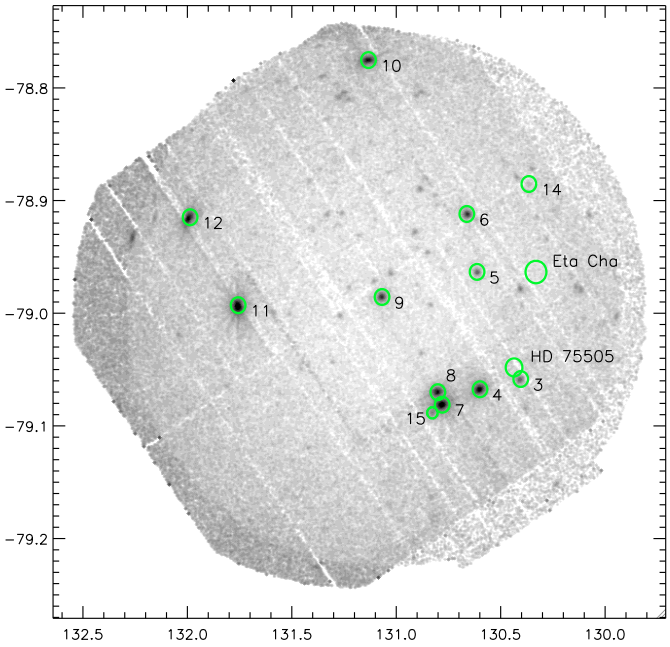

Fig. 1. EPIC-pn and mos mosaic of the η Chamaeleontis cluster. Known members of the cluster are marked with a circle and identified with its RECX number. The two members not detected in X-rays (η Cha and HD 75505) are identified with their most common name instead of their RECX identification (RECX 2 and RECX 13, respectively).

core of the cluster. This scenario was validated by Murphy et al. (2010), who identified four new probable cluster members and three possible members. With this new four stars, the census of known cluster members increases to twenty two (see Torres et al. 2008, for a review).

The proximity ($d \approx 97$ pc; Mamajek et al. 1999) and properties of η Chamaeleontis makes this cluster an ideal target for pointed X-ray observations. In this paper, we present a detailed study of the X-ray properties of cluster members based on a new deep *XMM-Newton* observation. Details of this observation are presented in Sect. 2 with the data reduction plan. In Sect. 3.1, we derive general coronal properties and attempt to relate them to other stellar properties such as binarity and the presence of accretion disks. X-ray variability (including flare-like variability) is studied in Sect. 3.2, where we also investigate the relation between flare energies and different stellar parameters. Section 4 is dedicated to other possible members in the field-of-view of our observation. Notes on particular sources are given in Sect. 5. Finally, in Sect. 6 we briefly summarize the main results of this work.

2. X-ray observation and data reduction

Our *XMM-Newton* observation of the η Chamaeleontis cluster (id. 0605950101) was performed in a single exposure of 48.3 ks on June 2009. The EPIC was used in full frame mode with the thick filter to reduce the contamination of the X-ray signal by visible and UV radiation. The effective exposure time of the observation was 46.4 ks in the EPIC-pn and 48.0 ks in the EPIC-mos. We performed a standard reduction using the version 9 of the specific *XMM-Newton* reduction package SAS. The observation was not affected by background flaring events and therefore, no time was lost by high X-ray variable background. For our study, we used a good-time-interval event file, i.e., cleaned of bad events and pixels, and noise. The image shown in Fig. 1 was created by constructing a combined EPIC-pn+mos image using the task EMOSAIC of the SAS. EPIC images were first individually corrected for the quantum efficiency, filter transmission, and mirror vignetting by dividing by the exposure maps obtained with the routine EEXMAP.

A modified version of the PWDetect code (Damiani et al. 1997) was used to detect sources in the 0.3−7.5 keV energy band. We chose the detection threshold $SNR = 5$, which corresponds to one possible spurious detection in each field as inferred from our simulations of the background in *XMM-Newton*[1]. With this threshold, a total of 86 sources were detected in the combined EPIC-pn and mos image. A direct visual inspection allowed us to discard 7 multiple detections (sources detected more than once by the detection algorithm) plus two spurious detections in the detector borders. The complete list of source detections is given in Table A.1. For each source, we indicate its position, significance of the detection, observed count-rate, and flux. This flux was determined by converting observed fluxes in photons cm^{-2} s^{-1} to erg cm^{-2} s^{-1} using the conversion factor $CF = 1.5 \pm 0.2 \times 10^{-9}$ erg ph^{-1}. This factor was determined from the spectral fitting of the known η Chamaeleontis members (see Sect. 3.1). We note that these fluxes are merely indicative. Most of the detected sources are active galactic nuclei instead of stellar coronae. This fact can be verified by comparing the fluxes determined for cluster members using the conversion factor (Table A.1) with the fluxes obtained from the spectral fitting (Table 2).

The value used by us as a detection threshold corresponds to a source count-rate limit of completeness $CR = 5.5 \pm 1.5 \times 10^{-4}$ s^{-1} in the EPIC energy band. Assuming a typical corona with $kT \sim 0.5$−1 keV, this count-rate corresponds to a flux $f_X \sim 1$−3×10^{-15} erg cm^{-2} s^{-1}, or $L_X \sim 2 \times 10^{27}$ erg s^{-1} at a distance of 100 pc (an upper limit to the distance of cluster members). This assures us that all the cluster members emitting

[1] We acknowledge Dr. I. Pillitteri for his help with the *XMM-Newton* background simulations.

Table 2. Spectral parameters of known members.

RECX	$N_{\rm H}$ ($\times 10^{21}$ cm^{-2})	kT_1 (keV)	kT_2 (keV)	kT_3 (keV)	EM_1/EM_2	EM_1/EM_3	Z ($Z_\odot$)	χ^2 (d.o.f.)	Unabsorbed $f_{\rm X}$ ($\times 10^{-13}$ erg cm^{-2} s^{-1})	log $L_{\rm X}$ (erg s^{-1})	log $L_{\rm X}$** (erg s^{-1})
3	$0.00^{+0.31}_{-0.00}$	$0.63^{+0.04}_{-0.04}$	...	...	...	...	$0.08^{+0.02}_{-0.02}$	1.12 (88)	$0.65^{+0.06}_{-0.10}$	28.9	29.2
4	$0.44^{+0.12}_{-0.11}$	$0.28^{+0.02}_{-0.01}$	$0.96^{+0.04}_{-0.03}$	...	0.92	...	$0.12^{+0.02}_{-0.01}$	1.29 (402)	$6.61^{0.71}_{2.97}$	29.9	30.2
5	$0.00^{+0.25}_{-0.00}$	$0.27^{+0.07}_{-0.06}$	$0.74^{+0.18}_{-0.09}$	...	1.30	...	$0.10^{+0.06}_{-0.03}$	0.96 (162)	$0.56^{+0.04}_{-0.12}$	28.8	29.1
6	$0.23^{+0.22}_{-0.19}$	$0.33^{+0.04}_{-0.03}$	$0.95^{+0.05}_{-0.06}$	...	0.88	...	$0.13^{+0.04}_{-0.03}$	0.93 (347)	$2.47^{+0.35}_{-0.20}$	29.4	29.6
7	$0.03^{+0.13}_{-0.03}$	$0.33^{+0.01}_{-0.01}$	$0.94^{+0.05}_{-0.04}$	$2.08^{+1.42}_{-0.36}$	0.75	2.21	$0.19^{+0.03}_{-0.04}$	1.03 (491)	$10.50^{+0.78}_{-0.50}$	30.1	30.4
8	$0.00^{+0.10}_{-0.00}$	$0.26^{+0.06}_{-0.03}$	$0.76^{+0.08}_{-0.06}$	$1.54^{+0.14}_{-0.13}$	0.87	0.61	$0.26^{+0.05}_{-0.05}$	1.28 (353)	$4.05^{+0.39}_{-0.31}$	29.7	29.9
9	$2.89^{+0.24}_{-0.29}$	$0.77^{+0.02}_{-0.04}$	$2.22^{+0.18}_{-0.18}$	...	0.47	...	$0.30^{+0.13}_{-0.06}$	1.12 (518)	$2.95^{+0.21}_{-0.38}$	29.5	28.5
10	$0.04^{+0.19}_{-0.04}$	$0.40^{+0.09}_{-0.04}$	$0.98^{+0.05}_{-0.06}$	...	0.72	...	$0.15^{+0.04}_{-0.04}$	0.92 (300)	$4.07^{+0.39}_{-0.31}$	29.7	30.0
11	$0.06^{+0.01}_{-0.01}$	$0.25^{+0.02}_{-0.01}$	$0.95^{+0.04}_{-0.04}$	$2.52^{+0.45}_{-0.27}$	0.90	1.20	$0.21^{+0.10}_{-0.05}$	1.20 (805)	$27.93^{+1.37}_{-2.83}$	30.5	30.2
12	$0.11^{+0.20}_{-0.11}$	$0.28^{+0.02}_{-0.02}$	$1.00^{+0.03}_{-0.03}$	$2.90^{+3.51}_{-0.99}$	0.73	2.45	$0.20^{+0.10}_{-0.09}$	...	$10.90^{+1.10}_{-0.58}$	30.1	30.2
14*	...	...	...	...	...	...	...	...	...	...	...
15	$1.27^{+0.47}_{-0.52}$	$0.80^{+0.18}_{-0.09}$	...	...	...	...	$0.04^{+0.02}_{-0.02}$	1.05 (64)	$0.31^{+0.07}_{-0.24}$	28.8	...

Notes. $^{(*)}$ The background subtracted spectrum of RECX 14 has only 67 counts. We failed any attempt of fitting a plasma model. $^{(**)}$ X-ray luminosities determined by Mamajek et al. (2000) in the 0.1−2.0 *ROSAT* energy band.

in X-rays have been detected. Compared to observations of other clusters and star-forming regions, our observation is one order of magnitude deeper in X-ray luminosities.

In Fig. 1, we mark with a circle the position of the known cluster members in the field of view of our observation. We note that two of them were not detected: the B star η Cha and the A star HD 75505 (see Sect. 5 for details).

3. General X-ray properties of η Chamaeleontis members

3.1. General properties

The fourteen known cluster members in the EPIC field of view include three early-type stars: η Cha (B8 V), HD 75505 (A0 V), and RS Cha (A7 V), and eleven Li-rich, H_α emission-line late-type (K6–M5) stars. The first X-ray characterization of this region was performed by Mamajek et al. (1999) based on pointed *ROSAT*-HRI [0.1−2.4 keV] broadband observations (see Sect. 1 for details). Unfortunately, those observations did not allow the authors to perform a complete spectral characterization of the detected sources, because of the limited spectral response of the HRI (see Mamajek et al. 2000). With the *XMM-Newton* [0.3−10 keV] observation, we are able to give parameters of the hot plasma by fitting plasma models to the X-ray spectrum of each star.

In our study, we assume that all the X-ray emission originates in the (hot) coronal plasma. This is accurate for non-accreting stars. However, it has been demonstrated that accretion shocks generate dense, relatively hot plasma that emits in very soft X-rays (e.g. Sacco et al. 2008; Brickhouse et al. 2010). Its contribution to the overall stellar X-ray emission is negligible in medium and hard X-rays ($kT \geq 0.5$ keV). However, when the accretion rate is high (about 10^{-10} $M_\odot$ yr^{-1}), the X-ray luminosity from the shocked plasma is the same order of magnitude than the typical X-ray luminosity of a T Tauri star (see Sacco et al. 2008). Of the four accreting stars in our sample, only one (RECX 15) has a high accretion rate (e.g. Sicilia-Aguilar et al. 2009). Nevertheless, it is highly absorbed in soft X-rays (see Table 2 and discussion below). Thus, the contribution of X-rays produced by the accretion to its spectrum is presumably very low, although high resolution observations would be needed to confirm this.

The EPIC spectra – integrated for the whole exposure – were analyzed using a 2T-temperature model. In some cases, a third temperature was added to obtain a robust fit at hard (i.e. above 2 keV) X-ray energies. We note here that the stars for which a 3-T model was used underwent flare-like events during the exposure (see Sect. 3.2). For them, we performed a more detailed study separating the quiescent from the flare state. The results of this study are shown in Table 4 and in Sect. 3.2. For the fit, we used the Astrophysical Plasma Emission Code (APEC, Smith et al. 2001a), which is part of the XSPEC spectral fitting package (Arnaud 1996, 2004). APEC is a routine that generates spectral models for hot (optically thin) plasmas using the atomic data contained in the Astrophysical Plasma Emission Database (APED, Smith et al. 2001b). We added a multiplicative interstellar absorption model in XSPEC – in particular the one described in Morrison & McCammon (1983) – to account for possible absorption due to interstellar and/or circumstellar material (for a more detailed description of the method we refer the reader to López-Santiago & Caballero 2008).

Best-fit parameters for the chosen models were found by χ^2 minimization and are shown in Fig. A.1. We note that the fits as given below are merely indicative. A 2-T model fitting to an observed coronal spectrum does not mean that we have to deal with two different plasmas at two different temperatures. In general, the coronal plasma exhibits a temperature gradient that cannot be studied using low-resolution X-ray spectra (although see Robrade & Schmitt 2005). Nevertheless, it has been shown that the dual-temperature nature of the fits may represent an intrinsic property of the coronal spectra of moderately active late-K and M stars (Schmitt et al. 1990; Briggs & Pye 2003; López-Santiago et al. 2007). In this scenario, the third (higher) temperature required to fit the hard tail of the X-ray spectrum is understood to be present only during flare-like events. In most cases, a successful 1-T model fitting is a mere reflection of a lack of information due to the low number of counts of many sources.

In Table 2, we present the best-fit parameters for each star. As a goodness-of-fit test, we give the reduced χ^2 and degrees of

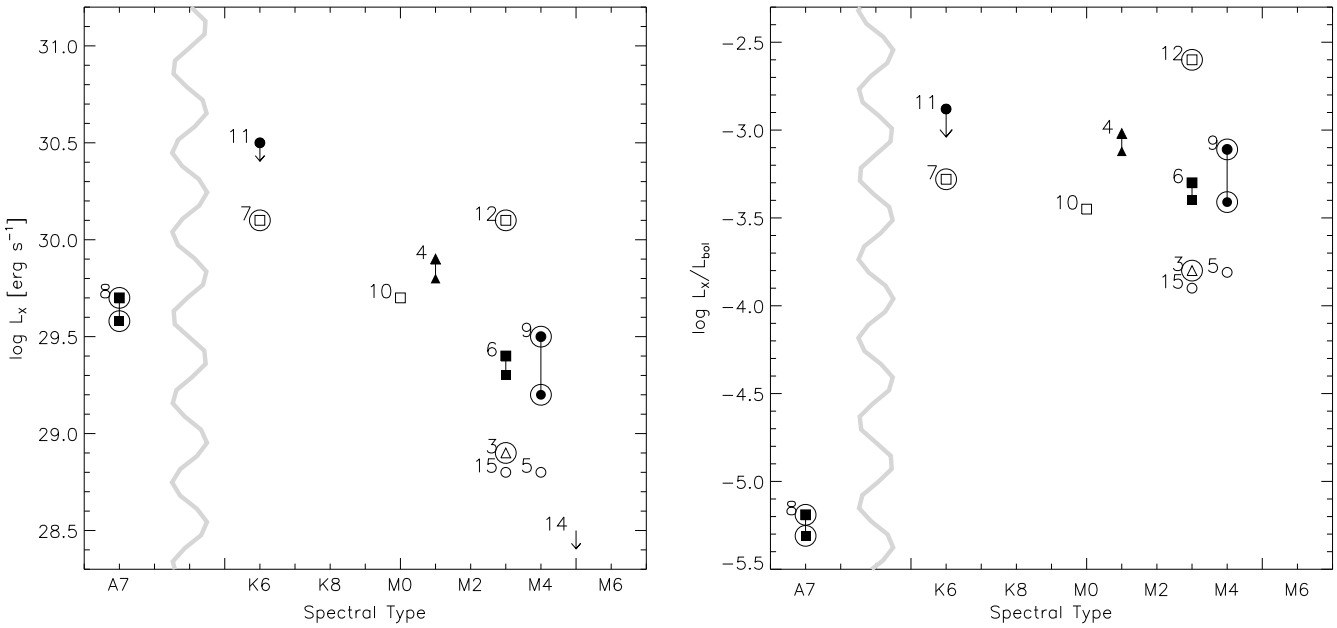

Fig. 2. X-ray luminosities of known members of η Chamaeleontis in the energy band 0.3−8.0 keV. Circles are known classical T Tauri stars, triangles are transitional objects, and squares are stars with no signatures of accretion disks. Filled symbols indicate stars that underwent a flare during our observation. Binary systems are marked with a large circle. Note that RECX 12 was observed, probably, in flare state during the exposure but was not clearly detected in its light curve because of its low count-rate (see Sect. 3.1).

freedom (d.o.f.) used for the fit. Unabsorbed fluxes in the energy band 0.3−8.0 keV are also given. Finally, the X-ray luminosities listed in the table were determined using the same distance for all the stars (d = 97 pc). It is noticeable that our luminosities are 0.2−0.3 dex lower than those determined by Mamajek et al. (2000) in a smaller energy range, except for EN Cha (RECX 9) and EP Cha (RECX 11) that underwent long duration flares during our exposure (see Sect. 3.2 and Fig. A.2). Nevertheless, it must be said that the authors could not perform model fitting to their data because of the poor spectral response of the *ROSAT*-HRI. Mamajek et al. (2000) then used a conversion factor to derive X-ray fluxes from the observed count-rates. In addition, they could not correct the observed fluxes for absorption. Taking all these factors into account, their estimations of the X-ray luminosities of the η Chamaeleontis members were quite reasonable.

The results presented in Table 2 for the coronal temperature should be interpreted with caution, since the X-ray spectra is affected by different influences. On average, the corona of the stars showing no flares during our observation are parametrized by a 2T-model with temperatures $kT_1 \approx 0.30$ keV and $kT_2 \approx 0.95$ keV. For stars that experienced a flare during the exposure, a third (hotter) component needs to be added to the model. For the two stars with lower count-rates (i.e. lower quality statistics) for which a 1T-model was used, the temperature obtained from the fit represents a mean value between kT_1 and kT_2, weighted by the emission measure. We refer the reader to López-Santiago et al. (2007) and Caballero et al. (2010) for a more detailed discussion of this issue. These results suggest that the X-ray spectrum of these stars during their quiescent state can be parametrized by a plasma model that is typical of both main- and pre-main-sequence stars. Only the star EN Cha (RECX 9) deviates from this trend ($kT_1 \approx 0.77$ keV, $kT_2 \approx 2.22$ keV). This is most likely because of the presence of absorbing material like a circumstellar disk (Sicilia-Aguilar et al. 2009), rather than the high X-ray emission produced during a flare-like event. We note that the star experienced a flare before the beginning of the exposure while we observed only the decay phase (see Fig. A.2), during which the plasma was rapidly cooling. The spectral analysis of the known cluster members inferred low mean column densities of $N_{\rm H} = 4.6 \times 10^{20}$ cm^{-2} and a typical deviation $\sigma = 8.5 \times 10^{20}$ cm^{-2}. The observed dispersion is due to the high $N_{\rm H}$ values found for the sources RECX 9 and 15. Both are well-known CTTS (e.g. Sicilia-Aguilar et al. 2009).

To investigate possible correlations between average X-ray luminosity and any stellar parameter, such as binarity, mass, or the presence of accretion disks, we used data from the literature (see Table 1). In Fig. 2, we plot different symbols for each object type (as classified by Sicilia-Aguilar et al. 2009): classical T Tauris (CTTSs, circles), transitional disk objects (TO, triangles), and weak-line T Tauris (WTTSs, squares). Filled symbols are stars with flare events during our observations. For these stars, we also plot the X-ray luminosity in the pseudo-quiescent state (see Sect. 3.2.1). Large circles mark binary stars. The upper-limit symbol used for RECX 11 denotes that its quiescent-state X-ray emission is probably lower than that determined from our observations. We assumed that the emission in the time-period $20 < t < 30$ ks is representative of the quiescent state of this star but this period is between two flare events (see Fig. A.2). No particular differences between the X-ray luminosity of binary and single stars or stars with and without an accretion disk is detected, although the sample is not large enough to extract any robust conclusion from this result. The typical trend of decreasing X-ray luminosity with decreasing mass (Preibisch et al. 2005) is observed. Nevertheless, the stars that underwent a flare during our observations have higher luminosities than stars with no flares, even when the contribution of the flare is subtracted. We note that EQ Cha (RECX 12) probably experienced a flare during the observations. A 3T-model with $kT_3 = 2.90$ keV was necessary for the fit (see Table 2). This difference in the X-ray luminosities for stars with similar spectral types may be explained by an enhancement of the X-ray emission (quiescent) level before the flares occur. This explanation should be interpreted with

caution, since the statistics in terms of numbers of stars is very poor.

3.2. X-ray variability

X-ray variability on a timescale of days was reported by Mamajek et al. (2000) for seven cluster members. The authors attributed this variability to flare-like events superimposed on moderately variable emission, but the poor signal for those observations prevented them from performing a quantitative analysis. In general, moderate variations on a timescale of a few days are probably due to rotational modulation (Marino et al. 2003). Examples of it are shown in Caballero et al. (2009) for the σ Orionis cluster and Flaccomio et al. (2005) for Orion. Flare-like events usually have short durations (of from a few minutes to a few hours) and involve a large release of energy. In young stars and particularly in T Tauri stars, they have been observed to have a large variety of shapes (e.g. Favata et al. 2005; Franciosini et al. 2007; López-Santiago et al. 2010). The *Chandra* and, in particular, the *XMM-Newton* missions owing to its large collector area, are powerful instruments for detecting flaring events in stars. In this sense, our observation is suitable for detecting short-time (<30 min) and medium-time (several hours) variations.

We extracted light curves from the EPIC-pn for the cluster members revealed in our observation, except for RECX 12, for which we used EPIC-mos since it was located in a gap between chips in the EPIC-pn. We chose a specific extraction radius for each source, depending on the position of the source at the detector, to avoid a loss of counts due to the degradation of the PSF towards the borders of the EPIC. A background region was chosen close to the source, in the same chip but far from other sources, and then subtracted from the source light curve. A different time binning was also used for each source depending on the source count-rate. The resultant background-subtracted light curves are shown in Fig. A.2. In Table 3, we provide details of the parameters for the extraction of the light curves (extraction radius and time binning), the type of variability detected and the count-rate increase factor during the flare in those stars in which a flare was clearly detected. We classified the type of variability as *flare*, when flare-like events were observed, or simply *variable*, for other types of variability. RECX 15 (ET Cha) is revealed above the background only in a small fraction of the exposure, around 30 ks from the beginning of the observation. We conclude that this star underwent a flare and that its quiescent emission is below the detection limit of this observation.

3.2.1. Flares

During the exposure time, five stars displayed clear flare activity (see Fig. A.2). Flares detected in our observation are not very intense in terms of count-rate enhancement (see Table 3). The count-rates were found to increase by factors of approximately 2–3, except for EN Cha (RECX 9). These values are similar to those observed in the less energetic flares detected in Taurus (Franciosini et al. 2007) and in M field stars (Robrade & Schmitt 2005; López-Santiago et al. 2007; Crespo-Chacón et al. 2007). In this sense, flares detected in members of η Chamaleontis are similar to those observed in other M-type stars.

We studied plasma parameters during the flares. In Table 4, we give the results of the fits of hot plasma models to the X-ray spectra of the stars during both the flare and the *quiescent* state for each star (assumed to be the characteristic level shown by the star previously to the flare, except for RECX 9, for which we used the last 6 ks of observation). As in the previous subsection, for the fit we used the XSPEC spectral fitting package with the APED and the WABS model (see Sect. 3.1). A 1T-model was used for the quiescent state, except for RECX 4 and RECX 11, for which it was necessary to add a second thermal component to fit the spectrum. We note that they are the sources with the higher mean count-rates. The goodness of the fit is given in the table as the reduced χ^2. For the flares, the fit was performed after subtracting the quiescent spectrum. An absorbed 1T-model was then used, maintaining the same values of $N_{\rm H}$ and Z as in the quiescent state. We note that temperatures obtained here are mean values, since we integrate over the entire event. The X-ray luminosities for the quiescent and the flare given in Table 4 are corrected for absorption. A mean distance of 97 pc was used to transform fluxes to luminosities for each star. The parameters $L_{\rm X}^{\rm fl}$ and $E_{\rm X}^{\rm fl}$ are, respectively, the X-ray luminosity and liberated energy during the flare event. Fluxes, luminosities and energies were determined in the [0.3–8.0] energy band. We note that our results for the flare parameters are relative to the pseudo-quiescent level chosen for the analysis. In particular, RECX 9 is observed during a flare decay phase and we adopted the last 8 ks of its exposure as its quiescent level. In general, the values obtained here for the flare energies are consistent with those found for members of Taurus (see below).

Table 3. Characteristics of the variations of the η Chamaleontis members.

Source	RECX	Ext. radius (arcsec)	Time bin (s)	Type	Factor	Flare dur. (ks)
EH Cha	3	15	1500			
EI Cha	4	15	900	Flare	2.7	>10
EK Cha	5	15	1200			
EL Cha	6	15	900	Flare	2.6	~4
EM Cha	7	15	900	Variable		
RS Cha	8	10	1000	Flare	1.8	~20
EN Cha	9	15	900	Flare	>7.3	>40
EO Cha	10	23	900	Variable		
EP Cha	11	32	900	Flare	1.4/1.7	~18/16
EQ Cha	12	32	1200	Flare?		
ES Cha	14	8	1200			
ET Cha	15	12	1800	Flare?		

Flare energies determined for our stars are typical of pre-main-sequence M stars. There seems to be no correlation with spectral-type, binarity, or the presence of disks. The energy liberated during the flare in RECX 6 (the only star with no sign of a disk among this group of stars showing flares) is one order of magnitude lower than for the others. However, this result is not conclusive because of the small sample we use. We compared our results with those obtained for the Taurus region by Stelzer et al. (2007). In Fig. 3, we plot the flare energies observed for the stars in our sample (triangles) with those in the *XMM-Newton* Extended Survey of the Taurus molecular cloud (XEST; plus symbols). Filled triangles and large symbols are used to mark stars with disks in our sample and the XEST one, respectively. Except for RECX 6 (with a flare energy $\log E_{\rm flare}$ [erg] = 32.6), the stars in our sample show flare energies similar to those in the XEST of the same spectral type. No difference between stars with and without disk is observed. The stars marked with a circle in Fig. 3 are classified as classical T Tauri in Güdel et al. (2007) and the stars marked with a square are embedded stars.

Table 4. Best-fit values of the spectral model parameters for the quiescent and the flare.

	Quiescent							Flare				
Source RECX	N_H ($\times 10^{21}$ cm^{-2})	Z ($Z_\odot$)	kT_1 (keV)	kT_2 (keV)	EM_1/EM_2	χ^2_q	log L^q_X (erg s^{-1})	kT_{fl} (keV)	EM_1/EM_{fl}	χ^2_{fl}	log L^{fl}_X (erg s^{-1})	log E^{fl}_X (erg)
4	$0.3^{+1.4}_{-0.8}$	$0.13^{+0.03}_{-0.02}$	$0.29^{+0.02}_{-0.02}$	$0.91^{+0.04}_{-0.04}$	0.99	1.10	29.8	$2.27^{+0.44}_{-0.48}$	0.77	1.07	29.9	>33.6
6	$0.0^{+0.2}_{-0.0}$	$0.08^{+0.02}_{-0.03}$	$0.73^{+0.04}_{-0.06}$	...	...	0.84	29.3	$3.17^{+24.8}_{-1.83}$	5.54	0.81	28.8	32.6
8	$0.3^{+0.4}_{-0.1}$	$0.05^{+0.03}_{-0.02}$	$0.74^{+0.08}_{-0.11}$	...	...	1.09	29.7	$1.05^{+0.33}_{-0.32}$	3.94	0.75	29.2	33.6
9	$1.6^{+0.4}_{-0.7}$	$0.13^{+0.13}_{-0.02}$	$1.24^{+0.37}_{-0.21}$	...	...	0.70	29.2	$1.54^{+0.35}_{-0.37}$	0.32	1.08	29.8	>34.4
11 (1st flare)	$1.0^{+0.2}_{-0.3}$	$0.12^{+0.04}_{-0.03}$	$0.26^{+0.02}_{-0.01}$	$1.21^{+0.06}_{-0.06}$	1.70	1.10	30.5	$2.12^{+1.08}_{-0.58}$	6.09	1.15	29.8	33.8
11 (2nd flare)	$1.0^{+0.2}_{-0.3}$	$0.12^{+0.04}_{-0.03}$	$0.26^{+0.02}_{-0.01}$	$1.21^{+0.06}_{-0.06}$	1.70	1.10	30.5	$1.49^{+0.55}_{-0.35}$	3.76	1.11	30.0	34.0

Notes. Errors correspond to the 90% confidence level. X-ray luminosities and flare energies are unabsorbed values. We assumed a distance of 97 pc for all the stars. Fluxes, luminosities, and energies were determined in the [0.3−8.0] energy band.

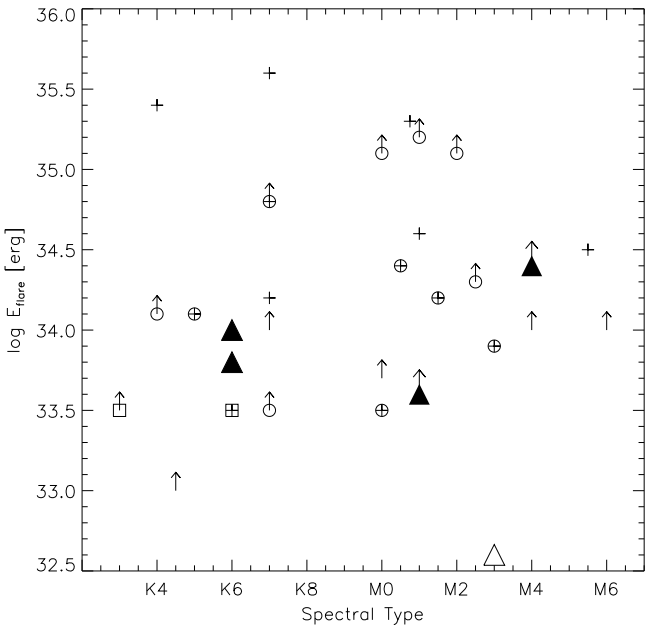

Fig. 3. Energy liberated during the flare in the [0.3−8.0] energy band for the stars in our sample (large triangles) and the stars of the XEST (plusses; Stelzer et al. 2007). Upward arrows denote lower limits. Filled triangles are stars with a disk in η Chamaleontis. Stars classified as classical T Tauri in Güdel et al. (2007) are marked with a large symbol (square or circle).

3.2.2. X-ray emission modulation

Six stars in our sample displayed some kind of modulation in their light curves during the observations. These stars have RECX numbers 6, 7, 10, 11, 12, and 15. In RECX 6 and RECX 11, the observed variations may be related to the decay of precedent flares. In particular, RECX 11 seems to exhibit two flares during the observing period. In the remaining stars, the variations may be related to rotational modulation.

The particular cases of RECX 7 and RECX 10 are interesting because they undergo a decrease in count-rate during a short period of time (~3 and 1.5 h respectively). This decrease could be related to an occultation of the corona by a companion. Of them, RECX 7 is known to be a double-line binary (Mamajek et al. 1999) with a period of 2.6 days (Lyo et al. 2003). However, RECX 10 has no known companion (Guenther et al. 2007).

4. Candidate cluster members in the field of view

Because of the low flux limit of our observation, we expected to detect all the cluster members emitting in X-rays in the EPIC field of view (see Sect. 2). Based on optical photometry, Mamajek et al. (2000) selected 50 candidates in the cluster core region. Lawson et al. (2002) confirmed that two low-mass stars inside the *ROSAT* field of view were members of η Chamaleontis using optical spectroscopy. They were not detected during the *ROSAT* observations. These two stars have RECX numbers 14 and 15 and were both detected in our observation (see Sect. 2 and Table A.1). The searching radius for candidates has been increased since then up to 5.5 deg (Luhman 2004; Lyo et al. 2004; Song et al. 2004; Lyo et al. 2006; Murphy et al. 2010). Six new members and 3 possible members have been identified at distances of between 1 and 6 deg from the cluster core. Most of these surveys were focused on identifying very low mass stars and brown dwarfs cluster members (e.g. Luhman 2004; Lyo et al. 2006; Murphy et al. 2010).

We searched for intermediate-mass (late-F and G type stars) members of the η Chamaleontis cluster that would not be detected by low-mass and brown dwarf surveys. Those stars should emit in X-rays with fluxes above our detection limit ($f_X \sim 1-3 \times 10^{-15}$ erg cm^{-2} s^{-1}; see Sect. 2). We first cross-correlated our X-ray sample with the 2MASS database (Skrutskie et al. 2006). A searching radius of 4 arcsec was used to prevent *false* positives in the identification. Della Ceca et al. (2004) estimated a positional error for the X-ray sources of the *XMM-Newton* Bright Serendipitous Survey of 6 arcsec. However, the mean distance between known members cluster and its X-ray counterpart in our observation is ~1.8 arcsec with a maximum separation of 2.8 arcsec for RECX 11. A searching radius of 4 arcmin is a conservative value.

The results of cross-correlating our X-ray sample with the 2MASS database are shown in Fig. 4. Small dots in the figure are 2MASS sources in the field of view of EPIC. Filled circles are the fourteen known cluster members in the same field of view. The twelve members detected in this observation are indicated by larger circles. Open circles are other X-ray sources in the field with a 2MASS counterpart. ZAMS and 8 Myr isochrone are also plotted. From these figures, only one of these other X-ray sources could be classified as possible members of the cluster. The star (2MASS J08483486-7853513) has the near-infrared colors of an M4/6 dwarf, which would correspond to a mass of 0.10−0.13 $M_\odot$ for a cluster member. However, Lawson et al. (2002) studied this star and found that it is likely to be a high-proper-motion dM5e foreground star at a distance of ~50 pc. The

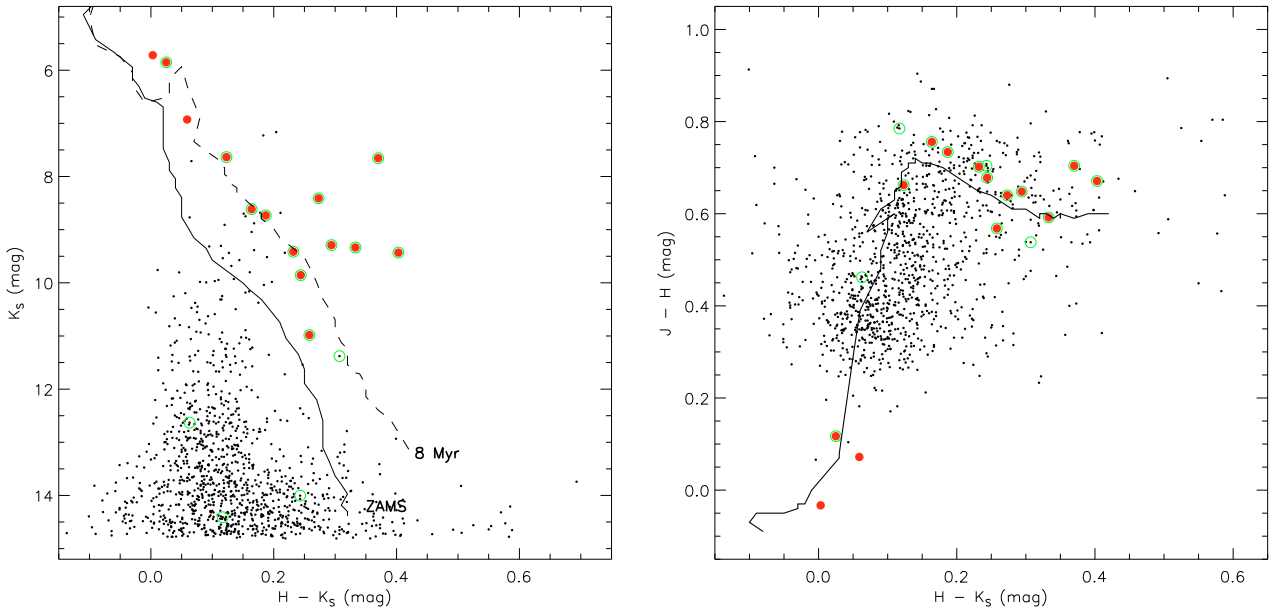

Fig. 4. 2MASS color−magnitude and color−color diagrams of the X-ray sources detected in the *XMM-Newton* image, plus η Cha. Filled circles are the known cluster members in the EPIC field of view. Those members detected in our observation are marked with a larger circle. Open circles are X-ray sources in our list of detections. Small dots are 2MASS sources in the field of view. ZAMS and 8 Myr isochrones are a combination of pre-main sequence models by Siess et al. (2000), for intermediate-mass stars and Baraffe et al. (1998), for low-mass stars. In the color-color diagram, we plot only the 8 Myr isochrone.

Table 5. Other X-ray sources in the field with 2MASS counterpart non-members of η Chamaleontis.

2MASS	J (mag)	H (mag)	K_S (mag)	Note
J08394669-7900026	17.21 ± 0.22	16.42 ± 0.22	15.56 ± 0.23	Galaxy
J08431595-7853422	14.95 ± 0.03	14.25 ± 0.04	14.00 ± 0.06	M-type
J08440921-7906156	15.31 ± 0.05	14.53 ± 0.06	14.41 ± 0.07	K-M giant
J08451844-7854426	13.16 ± 0.03	12.69 ± 0.02	12.63 ± 0.03	K-type
J08483486-7853513	12.22 ± 0.02	11.69 ± 0.03	11.40 ± 0.02	dM5e*

Notes. (*) Lawson et al. (2002) rejected this star as a cluster member and gave spectral type M5 with emission. Luhman (2004) later confirmed this result.

other three sources are background stars (see Fig. 4 and Table 5). We note that there is only one star in the field that could fulfill the requirement to be an intermediate-mass (FG-type star) cluster member in terms of near-infrared colors. This star is HD 76144. Nevertheless, the Hipparcos catalog gives a distance d = 140 pc, significantly larger than the value estimated for the cluster members. The star is not detected in the *XMM-Newton* observation with our detection procedure (see Sect. 2). We, therefore, also neglected this star as a member of η Chamaleontis.

5. Notes on individual stars

5.1. η Cha (RECX 2)

This star is the most massive cluster member (spectral type B8). It was detected by Mamajek et al. (1999) in a *ROSAT*-HRI observation. From the observed X-ray flux, they inferred an X-ray luminosity $\log L_X$ [erg cm^{-2} s^{-1}] = 28.8 in the HRI energy band. Mamajek et al. (2000) later suggested that η Cha is most likely a binary star, based on the observed variations in its radial velocity (Buscombe & Morris 1961). Therefore, they argued that the X-ray emission is likely to be produced in a low-mass secondary, for which Lyo et al. (2004) estimates a mass of 0.5 $M_\odot$ using $L_X - M$ relationships.

η Cha was not detected in our *XMM-Newton* observation. At our detection flux limit $f_X \sim 1{-}3 \times 10^{-15}$ erg cm^{-2} s^{-1} in the energy band [0.3−8.0] keV – which corresponds to a luminosity $L_X \sim 2 \times 10^{27}$ erg s^{-1} at a distance of 100 pc – any low-mass companion should have been detected (although see Sect. 3.2, where we suggest that ET Cha has a quiescent X-ray emission lower than the detection limit). The lack of X-ray emission from this star during the entire exposure cannot be simply explained in terms of variability. A possible scenario would be one in which the primary (non-emitting) star would eclipse the X-ray emitter for long periods of time. Nevertheless, that the X-ray emission would had gone unnoticed during this observation should not be disregarded. We note that ES Cha (RECX 14), the member with the lowest mass in the field of view, was observed at the detection limit. A lower mass star (spectral type later than M6) or even a brown dwarf may be part of this system. Any of these scenarios should be checked by performing a robust measurement of the system orbital parameters.

5.2. RS Cha (RECX 8)

RS Cha is a well-known Herbig Ae double-lined eclipsing binary with an orbital period P_{orb} = 1.67 days, located in the instability strip (Marconi & Palla 1998; Alecian et al. 2005). The pulsating nature of both stars in the system was confirmed by Böhm et al. (2009).

The X-ray emission detected with *ROSAT* by Mamajek et al. (1999) was proposed to come from a tertiary companion (Mamajek et al. 2000; Lyo et al. 2004). However, Alecian et al. (2005) found evidence that the time for the first conjunction of this system changes very rapidly with time, which is not expected if there is a third body in the system. The soft X-ray

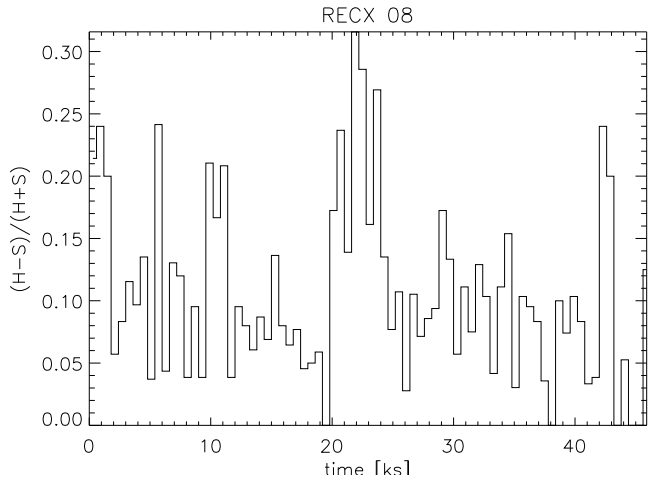

Fig. 5. Evolution of the hardness-ratio of RS Cha with time. The soft (S) and hard (H) energy bands are defined in the ranges [0.3−0.8] and [2.0−7.5] keV, respectively. Each bin is 10 min long.

emission may instead come from the A-type stars themselves, especially if they have disturbed atmospheres (Gómez de Castro 2009). But it has been shown that the X-ray spectral properties of Herbig Ae/Be stars are similar to those observed in the late-type stellar companions to other Herbig Ae/Be stars (e.g. Stelzer et al. 2006, 2009). The X-ray luminosity of RS Cha is indeed similar to that observed for the early-type M members of the cluster (see Fig. 2).

In the *XMM-Newton* observation, RS Cha underwent a flare, as confirmed by the temporal evolution of the spectrum hardness-ratio (Fig. 5). From the ephemeris for the primary minimum given by Clausen & Nordstrom (1980) and the linear variation in this relation with time observed by Alecian et al. (2005), we estimate that the primary eclipse finished ∼2.3 h after the beginning of the exposure, more than three hours before the flare occurred. Therefore, the shape of the light curve cannot be produced by an occultation of the X-ray emitter.

The flare temperature determined from the X-ray spectrum is quite low and the amount of material involved in the flare event is not large compared with the quiescent level (see Table 4). In this sense, the event detected in RS Cha is not very different from those observed in late-type cluster members as EP Cha (RECX 11).

5.3. EM Cha and EO Cha (RECX 7 and RECX 10)

During the observation, both stars exhibited a decrease in their count-rate by a factor of ∼1.5 during 3 and 1.5 h, respectively, in a way that resembles the occultation of part of the stellar corona by a companion (see Fig. A.2). EM Cha is known to be a binary star with a mass ratio of approximately 2.3:1 (Lyo et al. 2004). Following the results of Sect. 3.1, the low-mass companion may have an X-ray luminosity of 0.5−1 orders of magnitude lower than the primary (see Fig. 2). The occultation of part of the corona of the primary star by the secondary would produce a decrease of the observed total flux (i.e. of the observed count-rate). EO Cha, however, shows none sign of binarity (Guenther et al. 2007; Lyo et al. 2004). Therefore, the eclipse scenario does not seem probable for EO Cha.

The observed light curves may also be explained, in both cases, by the occultation of an active region behind the visible stellar hemisphere caused by stellar rotation. The count-rate of EO Cha increased over approximately 2.5 h before the rapid decrease during 1.5 h at the middle of the exposure. This fact may be interpreted as the occultation of an active region by the star's disk. Nevertheless, with the available data, neither of these two scenarios can be discarded.

5.4. EN Cha (RECX 9)

EN Cha is a classical T Tauri, binary system (Köhler & Petr-Gotzens 2002; Sicilia-Aguilar et al. 2009) formed by two nearly identical M-type stars (Mamajek et al. 2000; Lyo et al. 2004). During the *ROSAT* observation, this star was marginally detected above the background level, with an X-ray luminosity $\log L_X$ [erg cm^{-2} s^{-1}] = 28.5 (Mamajek et al. 2000). During the *XMM-Newton* observation, the star had a luminosity one order of magnitude higher than during the *ROSAT* observation.

From the light curve and coronal parameters obtained from the plasma model fitting (Fig. A.2 and Table 3), it seems clear that EN Cha underwent a flare during the *XMM-Newton* observation.

6. Summary and conclusions

We have presented a detailed study of the X-ray emission properties of the η Chamaeontis cluster members, based on a deep *XMM-Newton* observation toward the cluster core. This study is complete in terms of cluster members. We have detected all the (X-ray emitter) members of η Chamaeontis down to the sub-stellar mass limit. We have determined X-ray luminosities, coronal temperatures, abundances, and column densities from hot plasma model-fitting. Finally, we have also studied the variability of the sources.

The comparison between the X-ray luminosities derived in this work and those obtained by Mamajek et al. (2000) have shown that their values are overestimated, on average, by a factor of 2. The coronal properties determined for cluster members are typical of highly active stars. Multi-temperature models with at least two components were needed in the model-fitting. In the cases in which flare-like events were detected, a third hotter component was necessary to account for the enhancement of hard X-ray emission. In general, the stars that underwent a flare during our observations displayed higher pseudo-quiescent X-ray luminosities than members of similar spectral type that showed no flares. Six flares were detected in five of the cluster members with energies that are typical of pre-main- and main-sequence M stars. For these stars, coronal properties and X-ray luminosities were determined for the flare and the pseudo-quiescent states.

By comparing the X-ray luminosity of cluster members in different environments, i.e. with or without a protoplanetary disk in different evolutionary stages and binarity, we concluded that the only parameter that seems to influence the overall X-ray emission of the stars in η Chamaeontis is the spectral type. A similar conclusion can be made for the flare energies, although the sample of flare-like events during our observations is too poor for a robust conclusion to be made.

To complete our study, we searched for other cluster members in the field-of-view that might had gone unnoticed in previous surveys. We found five candidates, but discarded them as cluster members after a detailed study of their optical spectroscopic properties.

Acknowledgements. J.L.-S. and M.A.L.-G. acknowledge support by the Spanish Ministerio de Ciencia e Innovación under grant AYA2008-06423-C03-03.

J.F.A.C., is researcher of the CONICET and acknowledges support by grant PICT 2007-02177 (SecyT). We would like to acknowledge the anonymous referee for his/her useful comments on the text content.

References

Alecian, E., Catala, C., van't Veer-Menneret, C., Goupil, M.-J., & Balona, L. 2005, A&A, 442, 993
Arnaud, K. 1996, XSPEC: The First Ten Years, ed. G. H. Jacoby, & J. Barnes, ASP Conf. Ser., 101, 17
Arnaud, K. 2004, XSPEC: Progress and Plans, in the HEAD meeting, A&AS, 8, 16.29
Baraffe, I., Chabrier, G., Allard, F., & Hauschildt, P. H. 1998, A&A, 337, 403
Böhm, T., Zima, W., Catala, C., et al. 2009, A&A, 497, 183
Brickhouse, N. S., Cranmer, S. R., Dupree, A. K., Luna, G. J. M., & Wolk, S. 2010, ApJ, 710, 1835
Briggs, K. R., & Pye, J. P. 2003, MNRAS, 345, 714
Buscombe, W., & Morris, P. M. 1961, MNRAS, 123, 233
Caballero, J. A., López-Santiago, J., de Castro, E., & Cornide, M. 2009, AJ, 137, 5012
Caballero, J. A., Albacete Colombo, J. A., & López-Santiago, J. 2010, A&A, 521, A45
Clausen, J. V., & Nordstrom, B. 1980, A&A, 83, 339
Crespo-Chacón, I., Micela, G., Reale, F., et al. 2007, A&A, 471, 929
Damiani, F., Maggio, A., Micela, G., & Sciortino, S. 1997, ApJ, 483, 350
Della Ceca, R., Maccacaro, T., Caccianiga, A., et al. 2004, A&A, 428, 383
Favata, F., Flaccomio, E., Reale, F., et al. 2005, ApJS, 160, 469
Flaccomio, E., Micela, G., Sciortino, S., et al. 2005, ApJS, 160, 450
Franciosini, E., Pillitteri, I., Stelzer, B., et al. 2007, A&A, 468, 485
Frink, S., Roeser, S., Alcala, J. M., Covino, E., & Brandner, W. 1998, A&A, 338, 442
Gómez de Castro, A. I. 2009, ApJ, 698, L108
Güdel, M., Briggs, K. R., Arzner, K., et al. 2007, A&A, 468, 353
Guenther, E. W., Esposito, M., Mundt, R., et al. 2007, A&A, 467, 1147
Haisch, K. E., Jr., Jayawardhana, R., & Alves, J. 2005, ApJ, 627, L57
Jayawardhana, R., Coffey, J., Scholz, A., Brandeker, A., & van Kerkwijk, M. H. 2006, ApJ, 648, 1206
Köhler, R., & Petr-Gotzens, M. G. 2002, AJ, 124, 2899
Lawson, W. A., Crause, L. A., Mamajek, E. E., & Feigelson, E. D. 2002, MNRAS, 329, L29
López-Santiago, J., & Caballero, J. A. 2008, A&A, 491, 961
López-Santiago, J., Micela, G., Sciortino, S., et al. 2007, A&A, 463, 165
López-Santiago, J., Crespo-Chacón, I., Micela, G., & Reale, F. 2010, ApJ, 712, 78
Luhman, K. L. 2004, ApJ, 616, 1033
Lyo, A.-R., Lawson, W. A., Mamajek, E. E., et al. 2003, MNRAS, 338, 616
Lyo, A.-R., Lawson, W. A., Feigelson, E. D., & Crause, L. A. 2004, MNRAS, 347, 246
Lyo, A.-R., Song, I., Lawson, W. A., Bessell, M. S., & Zuckerman, B. 2006, MNRAS, 368, 1451
Mamajek, E. E., Lawson, W. A., & Feigelson, E. D. 1999, ApJ, 516, L77
Mamajek, E. E., Lawson, W. A., & Feigelson, E. D. 2000, ApJ, 544, 356
Marconi, M., & Palla, F. 1998, ApJ, 507, L141
Marino, A., Micela, G., Peres, G., & Sciortino, S. 2003, A&A, 406, 629
Megeath, S. T., Hartmann, L., Luhman, K. L., & Fazio, G. G. 2005, ApJ, 634, L113
Moraux, E., Lawson, W. A., & Clarke, C. 2007, A&A, 473, 163
Morrison, R., & McCammon, D. 1983, ApJ, 270, 119
Murphy, S. J., Lawson, W. A., & Bessel, M. S. 2010, MNRAS, 406, L50
Preibisch, T., Kim, Y.-C., Favata, F., et al. 2005, ApJS, 160, 401
Robrade, J., & Schmitt, J. H. M. M. 2005, A&A, 435, 1073
Sacco, G. G., Argiroffi, C., Orlando, S., et al. 2008, A&A, 491, L17
Sicilia-Aguilar, A., Bouwman, J., Juhász, A., et al. 2009, ApJ, 701, 1188
Siess, L., Dufour, E., & Forestini, M. 2000, A&A, 358, 593
Schmitt, J. H. M. M., Collura, A., Sciortino, S., et al. 1990, ApJ, 365, 704
Skrutskie, M. F., Cutri, R. M., Stiening, R., et al. 2006, AJ, 131, 1163
Smith, R. K., Brickhouse, N. S., Liedahl, D. A., & Raymond, J. C. 2001a, ApJ, 556, L91
Smith, R. K., Brickhouse, N. S., Liedahl, D. A., & Raymond, J. C. 2001b, Spectroscopic Challenges of Photoionized Plasmas, ASP Conf. Ser., 247, 161
Song, I., Zuckerman, B., & Bessell, M. S. 2004, ApJ, 600, 1016
Stelzer, B., Micela, G., Hamaguchi, K., & Schmitt, J. H. M. M. 2006, A&A, 457, 223
Stelzer, B., Flaccomio, E., Briggs, K., et al. 2007, A&A, 468, 463
Stelzer, B., Robrade, J., Schmitt, J. H. M. M., & Bouvier, J. 2009, A&A, 493, 1109
Torres, C. A. O., Quast, G. R., Melo, C. H. F., & Sterzik, M. F. 2008, Handbook of Star Forming Regions, Volume II, 757

Pages 10 to 13 are available in the electronic edition of the journal at http://www.aanda.org

Appendix A: On-line material

Table A.1. Sources detected in the 0.3–7.5 keV energy band using PWDetect with detection threshold *SNR* = 5.

Src #	Right Ascension (h m s)	Declination (° ′ ″)	Significance	Count-rate ($\times 10^{-3}$ s^{-1})	Observed flux* ($\times 10^{-13}$ erg cm^{-2} s^{-1})	Notes
1	08 45 33.9	–79 13 33.5	6.0	1.3 ± 0.7	0.09 ± 0.05	
2	08 42 42.8	–79 10 59.3	5.8	1.9 ± 0.3	0.14 ± 0.03	
3	08 44 07.3	–79 10 13.1	6.1	1.1 ± 0.2	0.08 ± 0.02	
4	08 43 19.7	–79 09 50.1	6.6	0.9 ± 0.2	0.07 ± 0.02	
5	08 40 53.4	–79 09 03.9	6.5	3.8 ± 0.4	0.29 ± 0.05	
6	08 45 42.3	–79 07 11.7	7.0	0.6 ± 0.1	0.04 ± 0.01	
7	08 44 9.4	–79 06 17.8	5.9	0.6 ± 0.1	0.04 ± 0.01	2MASS J08440921-7906156, field giant
8	08 42 10.8	–79 06 02.3	5.8	0.3 ± 0.1	0.02 ± 0.01	
9	08 43 18.4	–79 05 20.2	14.0	1.4 ± 0.2	0.10 ± 0.02	RECX 15
10	08 41 30.5	–79 05 02.9	8.1	0.7 ± 0.2	0.05 ± 0.01	
11	08 49 20.9	–79 04 50.9	5.6	1.0 ± 0.6	0.08 ± 0.05	
12	08 43 07.7	–79 04 53.9	244.9	131.9 ± 1.6	9.86 ± 1.32	RECX 7
13	08 42 49.6	–79 04 31.4	5.3	0.5 ± 0.1	0.03 ± 0.01	
14	08 43 12.5	–79 04 13.3	140.1	45.7 ± 1.0	3.41 ± 0.46	RECX 8
15	08 43 18.0	–79 04 10.6	5.7	0.3 ± 0.2	0.02 ± 0.02	
16	08 42 24.2	–79 04 04.6	170.4	67.3 ± 1.2	5.03 ± 0.68	RECX 4
17	08 47 15.0	–79 03 55.0	6.1	1.5 ± 0.2	0.12 ± 0.02	
18	08 41 37.2	–79 03 31.3	43.2	10.3 ± 0.5	0.77 ± 0.11	RECX 3
19	08 45 50.4	–79 02 58.0	7.2	0.5 ± 0.1	0.04 ± 0.01	
20	08 45 47.8	–79 02 38.4	6.1	0.2 ± 0.1	0.02 ± 0.01	
21	08 45 13.8	–79 02 37.2	9.9	0.8 ± 0.1	0.06 ± 0.01	
22	08 41 22.7	–79 02 33.0	6.9	0.9 ± 0.2	0.07 ± 0.02	
23	08 43 31.6	–79 02 08.3	14.0	1.0 ± 0.1	0.08 ± 0.01	
24	08 48 10.6	–79 01 05.9	8.7	1.5 ± 0.2	0.11 ± 0.02	
25	08 41 39.9	–79 00 55.7	5.5	0.2 ± 0.1	0.01 ± 0.01	
26	08 40 32.8	–79 00 45.8	5.7	0.7 ± 0.1	0.05 ± 0.01	
27	08 46 55.5	–79 00 17.7	5.1	0.3 ± 0.1	0.02 ± 0.01	
28	08 40 24.1	–79 00 12.0	5.7	0.6 ± 0.1	0.05 ± 0.01	
29	08 47 01.8	–79 00 11.4	5.8	0.4 ± 0.1	0.03 ± 0.01	
30	08 39 47.2	–79 00 04.6	11.2	2.0 ± 0.2	0.15 ± 0.03	2MASS J08394669-7900026, AGN
31	08 45 05.3	–79 00 09.3	16.9	1.3 ± 0.1	0.10 ± 0.02	
32	08 46 02.6	–79 00 01.0	7.7	0.6 ± 0.1	0.05 ± 0.01	
33	08 46 20.8	–78 59 58.2	6.0	0.5 ± 0.2	0.04 ± 0.02	
34	08 47 02.4	–78 59 36.5	320.1	251.6 ± 2.0	18.81 ± 2.51	RECX 11
35	08 41 36.3	–78 59 34.3	6.5	0.6 ± 0.1	0.04 ± 0.01	
36	08 43 20.7	–78 59 34.9	13.7	0.7 ± 0.1	0.05 ± 0.01	
37	08 44 17.1	–78 59 10.0	149.4	31.1 ± 0.5	2.33 ± 0.31	RECX 9
38	08 46 56.9	–78 58 55.5	5.8	0.4 ± 0.1	0.03 ± 0.01	
39	08 40 29.4	–78 58 41.0	15.4	2.9 ± 0.3	0.21 ± 0.04	
40	08 41 38.3	–78 58 41.3	32.2	5.3 ± 0.3	0.40 ± 0.06	
41	08 44 54.4	–78 58 38.6	12.1	0.6 ± 0.1	0.05 ± 0.01	
42	08 40 34.5	–78 58 31.4	10.6	1.0 ± 0.2	0.08 ± 0.02	
43	08 43 36.7	–78 58 29.4	6.9	0.3 ± 0.1	0.02 ± 0.01	
44	08 44 25.5	–78 58 18.9	14.5	1.1 ± 0.1	0.08 ± 0.01	
45	08 44 06.7	–78 57 53.4	21.2	3.1 ± 0.2	0.23 ± 0.03	
46	08 42 27.6	–78 57 49.5	58.7	8.3 ± 0.3	0.62 ± 0.09	RECX 5
47	08 43 24.5	–78 56 46.1	15.8	1.0 ± 0.1	0.07 ± 0.01	
48	08 43 36.1	–78 56 32.7	5.4	0.1 ± 0.0	0.01 ± 0.00	
49	08 41 09.0	–78 56 01.0	7.8	0.8 ± 0.1	0.06 ± 0.01	
50	08 49 01.1	–78 55 52.3	22.3	8.2 ± 1.3	0.62 ± 0.13	
51	08 44 42.3	–78 55 51.2	7.9	0.6 ± 0.1	0.04 ± 0.01	
52	08 43 39.0	–78 55 41.4	23.6	2.1 ± 0.2	0.16 ± 0.02	
53	08 45 36.0	–78 55 35.8	6.2	0.6 ± 0.1	0.05 ± 0.01	
54	08 48 01.1	–78 55 20.0	7.8	0.9 ± 0.2	0.07 ± 0.02	
55	08 47 57.4	–78 54 52.9	128.4	167.2 ± 1.7	12.50 ± 1.67	RECX 12
56	08 48 35.9	–78 54 50.0	10.7	2.3 ± 0.3	0.17 ± 0.03	
57	08 41 20.2	–78 54 49.4	7.9	1.6 ± 0.1	0.12 ± 0.02	
58	08 40 20.3	–78 54 42.3	11.1	3.6 ± 0.3	0.27 ± 0.04	
59	08 42 39.3	–78 54 43.7	116.1	27.0 ± 0.6	2.02 ± 0.27	RECX 6
60	08 45 19.6	–78 54 43.8	10.7	0.9 ± 0.2	0.07 ± 0.02	

Table A.1. continued.

Src #	Right Ascension (h m s)	Declination (° ′ ″)	Significance	Count-rate ($\times 10^{-3}$ s^{-1})	Observed flux* ($\times 10^{-13}$ erg cm^{-2} s^{-1})	Notes
61	08 45 01.9	–78 54 40.4	11.9	1.0 ± 0.1	0.08 ± 0.01	
62	08 47 52.2	–78 54 16.4	6.2	0.5 ± 0.1	0.03 ± 0.01	
63	08 43 13.7	–78 54 14.5	6.5	0.5 ± 0.1	0.04 ± 0.01	
64	08 44 29.9	–78 54 03.5	5.3	0.2 ± 0.0	0.01 ± 0.00	
65	08 48 35.4	–78 53 48.4	5.9	1.6 ± 0.4	0.12 ± 0.04	2MASS J08483486-7853513, field dM5e
66	08 43 16.6	–78 53 44.1	7.6	0.5 ± 0.1	0.03 ± 0.01	2MASS J08431595-7853422, field M
67	08 43 33.4	–78 53 24.0	24.2	2.6 ± 0.2	0.19 ± 0.03	
68	08 39 47.4	–78 53 01.4	36.2	22.5 ± 11.3	1.68 ± 0.88	
69	08 41 29.9	–78 53 05.2	5.1	0.6 ± 0.1	0.04 ± 0.01	RECX 14
70	08 45 08.9	–78 53 03.5	5.7	0.2 ± 0.1	0.02 ± 0.00	
71	08 45 39.8	–78 52 58.3	8.4	1.1 ± 0.2	0.08 ± 0.02	
72	08 41 43.0	–78 52 42.9	12.5	1.4 ± 0.2	0.11 ± 0.02	
73	08 41 26.1	–78 52 16.5	11.5	1.2 ± 0.2	0.09 ± 0.02	
74	08 47 39.1	–78 50 36.0	6.8	1.2 ± 0.2	0.09 ± 0.02	
75	08 47 52.1	–78 50 10.4	8.2	0.8 ± 0.2	0.06 ± 0.01	
76	08 45 18.5	–78 49 40.9	5.7	0.9 ± 0.2	0.07 ± 0.02	
77	08 44 54.2	–78 48 36.9	9.9	1.1 ± 0.2	0.08 ± 0.02	
78	08 45 04.5	–78 48 28.3	14.4	3.1 ± 0.3	0.23 ± 0.04	
79	08 43 37.7	–78 48 25.5	8.0	0.8 ± 0.2	0.06 ± 0.01	
80	08 44 59.8	–78 48 15.8	11.7	2.1 ± 0.3	0.16 ± 0.03	
81	08 43 32.2	–78 48 13.4	10.6	0.9 ± 0.2	0.07 ± 0.01	
82	08 45 53.2	–78 47 59.2	7.4	2.3 ± 0.3	0.17 ± 0.03	
83	08 46 14.0	–78 47 39.0	5.4	1.0 ± 0.2	0.07 ± 0.02	
84	08 45 23.7	–78 47 23.8	11.3	2.6 ± 0.3	0.19 ± 0.03	
85	08 44 32.2	–78 46 31.7	88.5	41.3 ± 1.4	3.09 ± 0.42	RECX 10
86	08 45 27.8	–78 45 45.4	5.7	1.0 ± 0.2	0.07 ± 0.02	

Notes. (*) Observed fluxes determined using the conversion factor $CF = 1.5 \pm 0.2 \times 10^{-9}$ erg ph^{-1}. Fluxes from the spectral fitting for the known cluster members are given in Table 2.

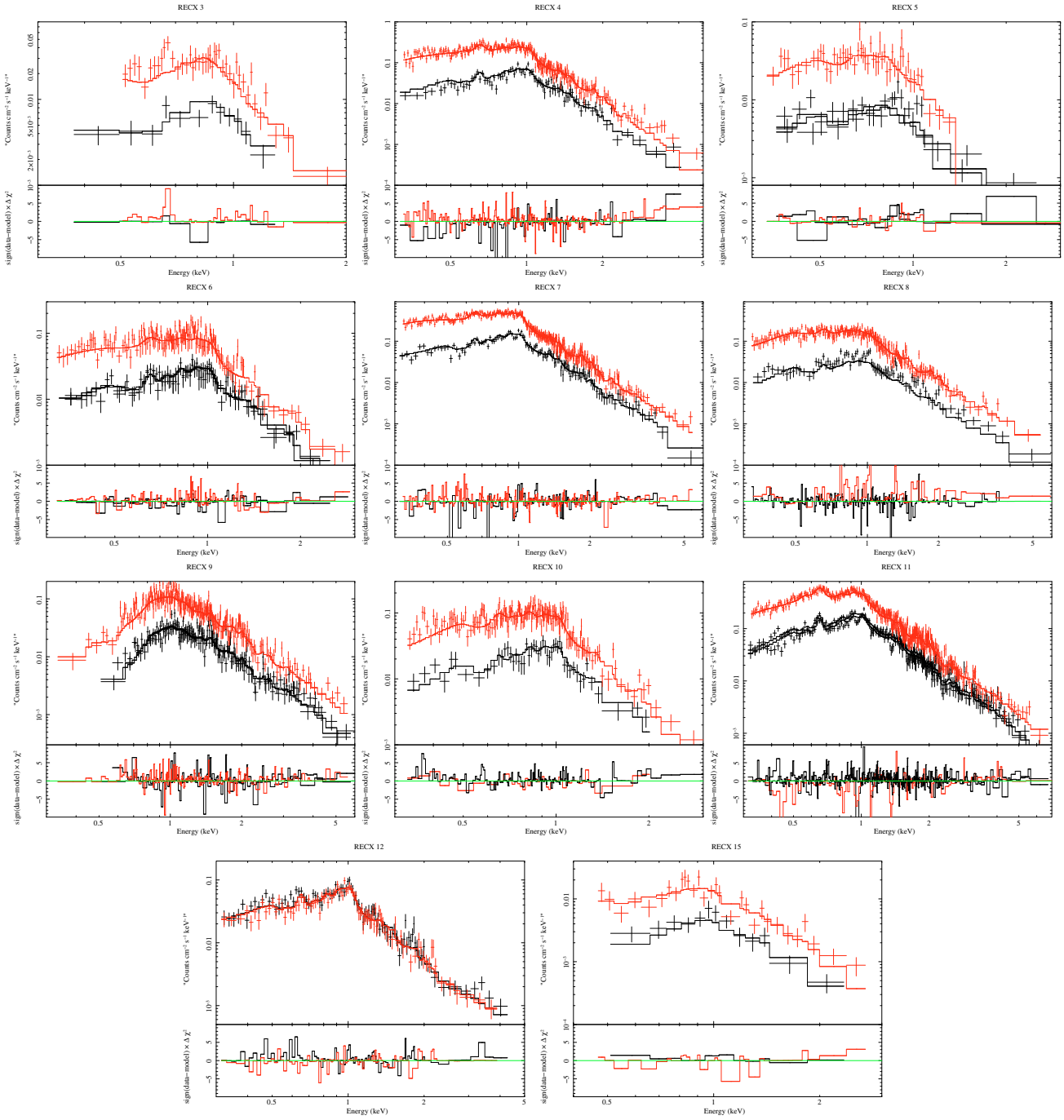

Fig. A.1. X-ray spectra for known members of η Chamaleontis. Red is for EPIC-pn and black is for EPIC-mos, except for RECX 12 that is located in an EPIC-pn gap. The best fit to each spectrum is also plotted. The *bottom panel* represents the deviation of the model from the observed spectra in each spectral bin.

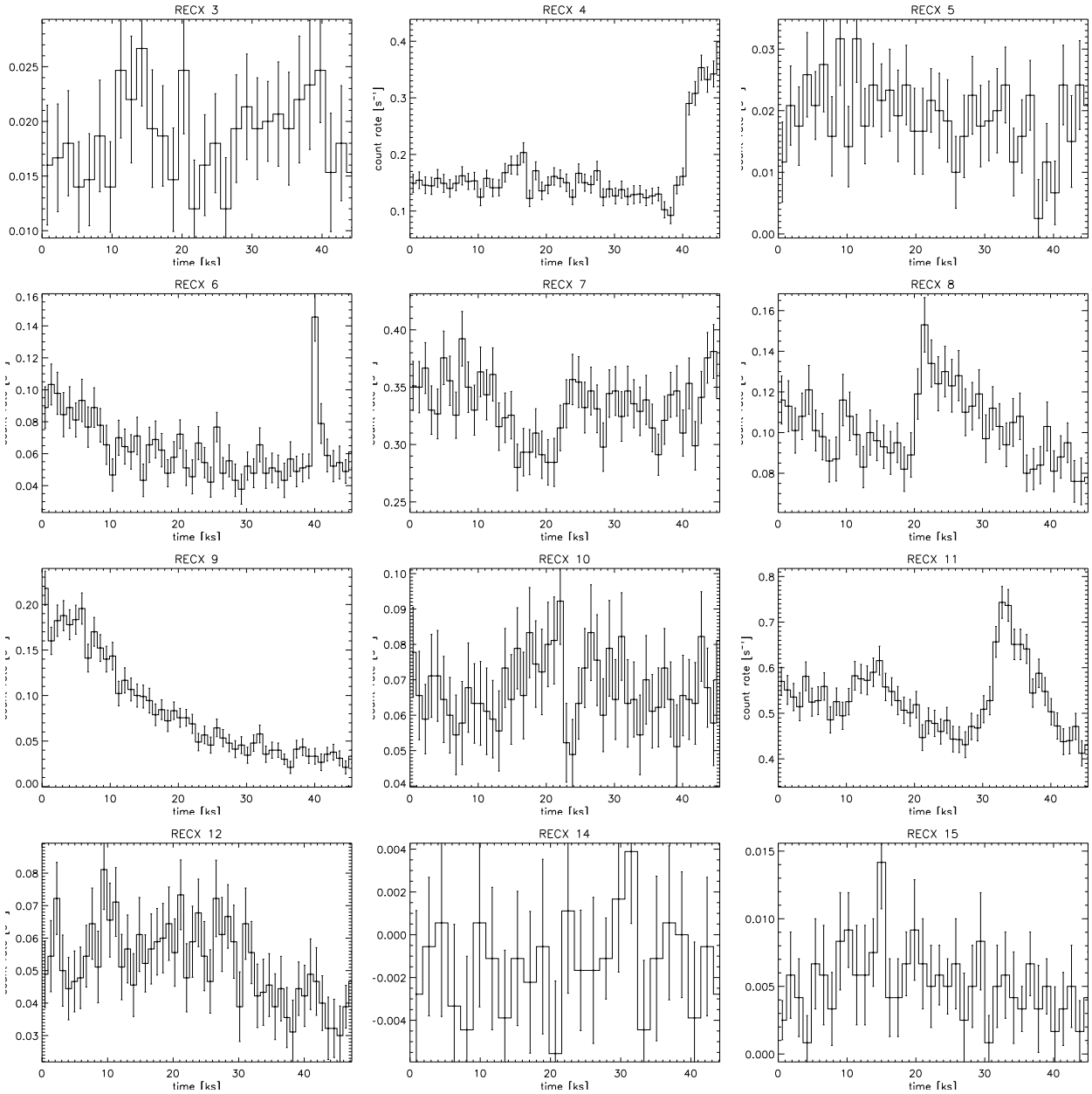

Fig. A.2. X-ray light curves in the energy band 0.3−8.0 keV for known members of η Chamaleontis. Time binning ranges from 15 to 30 min.